Distance and potential dependence of charge transport through the P700 reaction center of Photosystem I

Manuel López-Ortiz[1,2], Ricardo Zamora-Brito[1,2], Marina Inés Giannotti,[1,2,3] Chen Hu[4], Roberta Croce[4], Pau Gorostiza[1,2,5,*]

1. Institute for Bioengineering of Catalonia (IBEC), The Barcelona Institute of Science and Technology, Baldiri Reixac 10–12, Barcelona 08028

2. Network Biomedical Research Center on Bioengineering, Biomaterials and Nanomedicine (CIBER-BBN), Madrid 28029

3. Department of Materials Science and Physical Chemistry, University of Barcelona, Martí i Franquès 1-11, Barcelona 08028

4. Biophysics of Photosynthesis. Dep. Physics and Astronomy, Faculty of Sciences, Vrije Universiteit Amsterdam, De Boelelaan 1081, 1081 HV Amsterdam

5. Catalan Institution for Research and Advanced Studies (ICREA), Barcelona 08010

** E-mail: pau@icrea.cat*

Abstract

Photoinduced charge separation and transport through photosystem I (PSI) is an essential part of the photosynthetic electron transport chain. To investigate charge exchange processes mediated by the P700 reaction center of PSI, we have developed a strategy to functionalize gold electrodes with PSI complexes that orients and exposes their luminal side to the electrolyte. Bulk photoelectrochemical measurements demonstrate that PSI remains functional in a wide sample potential range around 0 mV/SSC. Electrochemical scanning tunneling microscopy (ECSTM) imaging of individual complexes shows lateral sizes in agreement with the dimensions of PSI and an apparent height that is gated by the probe potential of ECTSM as reported for smaller globular redox proteins. This experimental setup enables ECSTM current-distance spectroscopic measurements that unequivocally correspond to the P700 side of PSI. In these conditions, we observe that the spatial span of the current is enhanced (the distance-decay rate β is reduced) through the solution at sample potential 0 mV/SSC and probe potential 400 mV/SSC. This process corresponds to hole injection into an electronic state that is available in the absence of illumination. We propose that a pair of tryptophan residues located near P700 and known to integrate the hydrophobic recognition site for plastocyanin may have an additional role as hole exchange mediator involved in charge transport through PSI.

Introduction

Electron Transfer (ET) is a charge exchange process driven by the difference in redox potential between donor an acceptor species. In biology, ET is an essential component of the electron transport chains involved in cellular respiration and photosynthesis. ET in the photosystem I (PSI) complex has been extensively studied[1] both for basic and applied purposes. PSI is a light-driven oxido-reductase that transfers electrons from the luminal to the stromal side of the thylakoid membrane embedding the complex[2]. This transfer is the result of subsequent ET processes between the cofactors integrating PSI and its partner proteins(Figure 1). Thisis an energetically uphill process powered by the excitonic energy harvested by the pigments found in the reaction center and in the light harvesting complex (LHCI) associated to PSI.[3,4] The combination of efficient excitonic energy transfer[3] and fast ET (10^{-8} – 10^{-7} s)[4] results in a quantum yield near unit for the PSI electron transport chain. This efficiency figure of merit is often used to highlight the potential of PSI in biohybrid solar energy harvesting.[5–7] Upon light irradiation, PSI complexes are brought to a long-lived state formed by a pair of spatially and energetically distant redox cofactors (Figure 1): the photo-oxidized $P700^+$ (270 mV/SSC)[8] in the luminal side is an electron acceptor located 5 nm away from the terminal electron donor, the reduced iron sulfur F_b^- in the stromal side. Thus, for irradiated PSI complexes in physiological conditions, electrons flow from P700 to F_b.

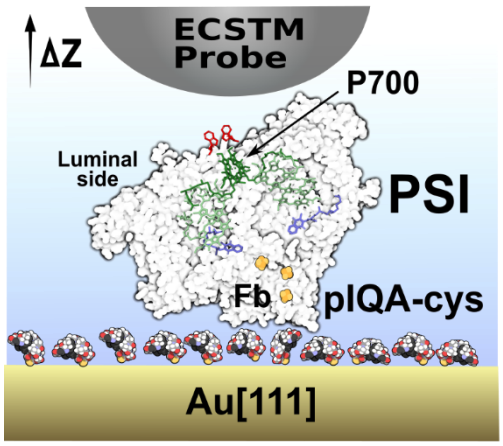

Figure 1. Scheme of the molecular arrangement set up in this work to attach and orient PSI complexes on Au[111] atomically flat electrodes. Peptides recognizing PSI stromal side with a C-terminal cysteine residue (pIQA-cys) were attached to the gold surface in order to bind plant PSI complexes.[2121] This functionalization exposes the P700 site (luminal side) to the solution, enabling reproducible bulk photoelectrochemical measurements as well as single molecule measurements like scanning probe microscopy and spectroscopy. An electrochemical scanning tunneling microscopy (ECSTM) probe electrode is depicted on top of the PSI complex (reference and auxiliary electrodes are not shown for simplicity). The electrochemical potential and position (z) of the probe can be accurately controlled during charge exchange with the P700 site.

Monitoring the ET of individual redox proteins allows singling out their contribution to the ensemble current and has been enabled by *in situ* scanning probe techniques along with methods to specifically connect proteins to planar conductive electrodes[9]. Electrochemical scanning tunneling microscopy (ECSTM) studies of several metalloproteins[9–13] have revealed a current enhancement or gating effect (see below) as the Fermi levels of the sample/probe electrode pair align with the molecular orbitals of the protein. In protein junctions where the macromolecule contacts both electrodes, the charge exchange is driven by the potential drop between the electrodes rather than by the redox potential responsible for ET[14]. This charge exchange mechanism through a biased electrode, known as electron transport (ETp) can be achieved in ECSTM (break junction and blinking modes), conductive atomic force microscopy (C-AFM), liquid metal contacts, microfabricated gold nano wire set-ups[15]. A growing amount of evidence[14,16–18] shows that ETp is a ubiquitous charge conduction mechanism through the protein matrix, and that it confers conductivities to redox and non-redox proteins outperforming molecular wires beyond 5 nm distances[19]. Although the physiological relevance of ETp through protein junctions is less studied than that of ET, understanding protein ETp is key to engineer protein-based electronic devices[14,20].

In particular, ETp through PSI complexes in the dark, evidenced by the current rectifying behavior of oriented PSI monolayers[21,22] is favored in the stroma-to-lumen direction (from F_b to P700) following the PSI natural dipole[23]. That is, in the dark the preferred sense of ETp in PSI is against the physiological direction.Despite the differences between redox ET and ETp observed in proteins, a common ground under both processes has been proposed[14,24]. As a first step to link these processes we have chosen to study the behavior of PSI under dark conditions (non-redox active state) and we have applied potentials to favor currents in the sense of PSI ETp.

An exponential decay of the charge exchange rate with the distance is observed between the donor and the acceptor in ET and between the protein and the electrodes in ETp. This is due respectively to the electronic coupling between donor and acceptor molecular orbitals, and between the electrode Fermi level and the protein molecular orbital. Experimentally, the distance decay rate β [nm^{-1}] of the ET between a prosthetic ruthenium atom and the copper center in Ru-modified Azurin mutants[25,26] yields 11 nm^{-1}. For Azurin functionalized in gold electrodes with alkanethiol of different lengths,[27] a value of $\beta = 1.03 \pm 0.02$ nm^{-1} per CH_2 is found. In an ECSTM setup β can be directly evaluated from current vs distance curves[28]. In this case, β accounts for the distance decay resulting from all charge exchange processes between the protein-functionalized sample and probe electrodes. For instance, the β value for bare gold electrodes in physiological medium is 10 nm^{-1}. In gold electrodes functionalized with azurin proteins[28], β is 4 nm^{-1} and similar β values have been obtained for DNA base pairs[29] and redox proteins. [30,31] Moreover, β depends on potential and is lowest (current is most enhanced) where the electrode Fermi level is near the redox level of the protein[28,30,31] or redox-active organic compound[32]. Our previous results with PSI complexes[30] suggest that long distance charge transport is electrochemically gated[30]. In that work we used thiolated self-assembled monolayers (SAM) exposing a negatively charged surface, which have been largely employed for PSI immobilization[33]. The present study aims to determine the distance and potential dependence of ET/ETp through the P700 reaction center of PSI and thus requires better defined protein orientation, and higher recognition specificity.

PSI orientation has been inferred from the current-rectifying behavior of SAM-PSI monolayers evaluated with STM[34] and C-AFM[35]. The heterogeneous but still preferential orientation of PSI molecules was attributed to SAM-PSI electrostatic interactions[33]. Specific binding and orientation of cyanobacterial PSI complexes to ITO electrodes was achieved by *Gordiichuk et al.* via a synthetic peptide (pIQA)[22] that binds to the stromal side of cyanobacterial PSI from *Thermosynechococcus elongatus*. PSI orientation was evaluated from the current-rectifying behavior of the PSI-pIQA-ITO monolayer. To investigate the charge exchange process with the P700 site in PSI, here we have designed a pIQA derivative to bind and orient plant PSI complexes on atomically flat gold electrodes. We reasoned that the pIQA structure would be recognized by the plant PSI due to its high homology with cyanobacterial PSI complexes. We modified pIQA peptide for Au substrate attachment by introducing a cysteine (pIQA-cys.[22] The resulting PSI-pIQA-cys-Au functionalization yields robust macroscopic photocurrents in a wide potential window and enables reproducible high-resolution microscopy and spectroscopy of individual PSI complexes. In these conditions, the charge exchange between the P700 site exposed to the solution and the ECSTM probe reveals long distance dependence (low β) and electrochemical gating. The results are in agreement with hole injection into PSI and reveal the presence of a low-energy state in the absence of illumination.

Results and discussion

Topography of oriented PSI on Au by scanning probe microscopy: AFM of PSI-pIQA-cys-Au[111] electrodes (Figure 2a-c) shows the presence of a homogeneous sub-monolayer of 6 nm thickness, which is in agreement with previously reported PSI assemblies on gold[36,37] (see experimental section and Suppl. Figure S1). The lateral size of PSI single particles was not determined due to limited AFM probe resolution. Single complex resolution is achieved in ECSTM image (Figure 2d-e). For each complex, long and short axes in the horizontal plane were fit with a 2D-gaussian model (Suppl. Figure S3). Size distribution for N=334 particles yields 6.5 ± 0.1 nm and 10.7 ± 0.3 nm for short and long axes respectively. Protein lateral sizes, taken as full width at half maximum, are 60% and 70% smaller respectively than available crystallographic structure of PSI-LHCI structure[38], with an approximate size of 10.5 nm and 15 nm.

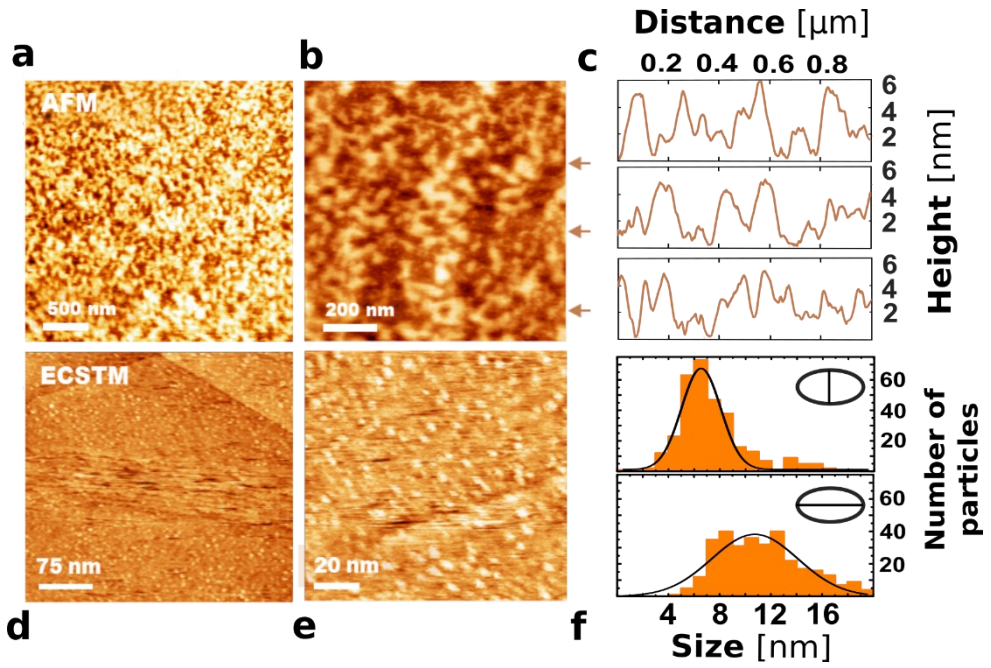

Figure 2. Structural characterization of of PSI-pIQA-cys films attached to atomically flat Au[111] electrodes. AFM image of PSI-pIQA-cys-Au[111], scan size 3x3 µm **a.** and 1x1 µm **b**. The vertical (z) color scale is set to 8 nm amplitude. **c.** Example AFM height profiles at the positions indicated with arrows in panel (b). ECSTM images of the same sample, 350x350 nm **d**. and 150x150 nm **e**. The vertical (z) color scales correspond to 1.4 nm and 1.1 nm respectively. The set point tunnel current is 0.2 nA and the bias is 300 mV (U_S = 0 mV/SSC, U_P = 300 mV/SSC). **f.** Distribution of ECSTM particle size, short axis (top) and long axis (bottom).

Electrochemical potential dependence of PSI-pIQA-cys-Au[111] microscopy and photocurrent recordings: The topography (apparent height) of PSI monolayers observed by ECTSM (Figure 3a) is tenfold lower than that observed by AFM (Figures 2ab). This result agrees with previous reports about PSI complexes on alkanethiol-functionalized gold substrates.[30] Since ECSTM is operated in constant current feedback mode, the apparent height is due both to the topography and to the conductance of the sample. ECSTM apparent heights lower than the known structural dimensions have been observed for several proteins deposited on metal substrates.[27,39–43] These results confirm that protein conductance is larger than that of the surrounding electrolytic medium, both in metalloproteins[44–46] and interestingly in non-redox active proteins.[16,17] In addition, we observe that the apparent height of PSI complexes by ECSTM depends on the probe potential U_P (Figure 3a). This effect allows using ECSTM imaging at different electrochemical potentials to study their conductance and charge transport properties. Several works showed a similar dependence in the small globular protein azurin,[13, 12] and more recently in a 100 kDa

oxidoreductase complex[47]. This gated conductance resonance is attributed to the alignment of the Fermi levels of the ECSTM sample and probe electrodes with the redox energy (molecular orbital) of the molecule under study.

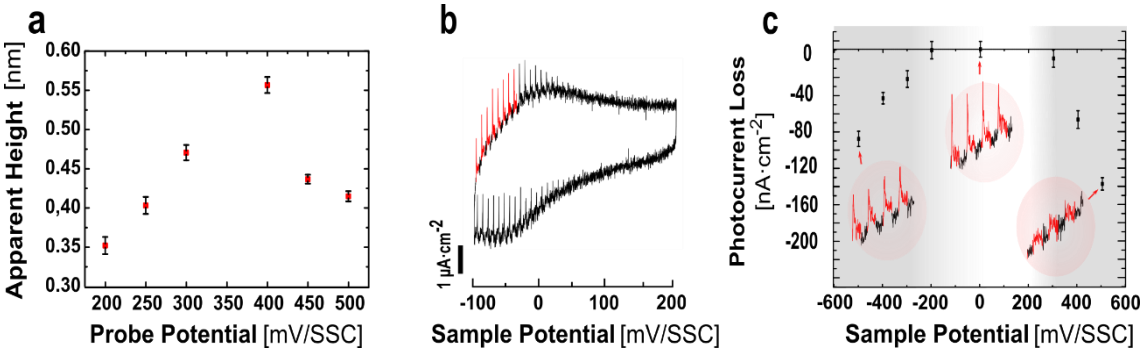

Figure 3. Dependence of PSI-pIQA-cys-Au microscopy and photocurrent recordings on the electrochemical potential: a. Apparent height of PSI complexes measured from ECSTM image profiles at different probe potentials U_P (constant bias potential $U_{bias} = U_P - U_S =$ 300 mV/SSC). A maximum PSI height is observed at U_P = 400 mV/SSC indicating a conductance resonance as observed for redox proteins and complexes. **b.** Bulk photoelectrochemical current measured in a PSI-pIQA-cys-Au sample during cyclic voltammetry at 80 mV/s rate while switching on and off the 690 nm illumination every 125 ms (red and black traces, respectively). Photoresponses are observed at U_S < 100 mV/SSC. **c**. An electrochemical potential window of PSI stability between -200 and +300 mV/SSC is identified where photocurrent loss is below 10% (white band and example photocurrent recording at the center, red traces corresponding to 690 nm illumination). Applying potentials outside this window diminishes photoresponses (indicated by grey bands and example photocurrent traces).

The activity of PSI-pIQA-cys-Au samples was tested with photo-chrono-amperometry before current decay spectroscopy experiments, acquiring photocurrents of 10 nA·cm^{-2} at U_S = -100 mV/SSC (Suppl. Figure S4). To define a working electrochemical window, chopped light cyclic voltammetry experiments (Suppl. Figures S5-6) were performed. Soluble redox mediators methyl viologen (125 µM) and osmium bipyridine dichloride (10 µM) were added to the buffer solution to enhance photocurrents and facilitate the characterization.[37] Illuminating PSI complexes at U_S = -100 mV/SSC produces photocurrents with 1 µA·cm^{-2} transient and 200 nA·cm^{-2} steady components. Photocurrents depend on the applied sample potential and can only be reversibly measured below 100 mV/SSC. Potential excursions within the range -200 mV/SSC to 300 mV/SCC do not alter the magnitude of photocurrents, but they are reduced after applying potentials outside this "safe" electrochemical window (Suppl. Figures S5-S6). The photocurrent loss (Figure 3c) was estimated comparing photocurrents measured in a reference potential region between -100 mV/SSC and -25 mV/SSC (indicated by red traces in Figure 3b) before and after applying a test potential during 5 min (Suppl. Figure S5-S6). For potentials U_S < -200 mV/SSC, cathodic currents increase significantly due to the presence of O_2 in the electrochemical cell.[48–50] After applying U_S = -400 mV/SSC for 5 min (Suppl. Figure S5), the voltammogram is broadened indicating a decrease of the electrode capacity revealing a partial depletion of absorbed molecules. A decrease in photocurrent amplitude is also observed. Photocurrent degradation has been attributed to the formation of ROS in aerobic systems where O_2 acts as terminal electron acceptor.[48,49] Similar irreversible decrease of photocurrent and electrode capacity is observed for positive potentials outside the safe window (U_S > 300 mV/SSC). Reversible and stable photocurrent measurements in the electrochemical window between -200 mV/SSC < U_S < +300 mV/SSC indicate the presence of functional (photo-active) PSI complexes in the electrode. We took these values to set the sample potential boundaries to study single PSI spectroscopy with ECSTM in the dark.

Thus, in Figures 2 and 3 the microscopic and bulk photocurrent characterization of PSI-pIQA-cys functionalized gold electrodes show: (i) sub-monolayer coverage of PSI complexes, (ii) conductance gating in the PSI apparent height measured by ECSTM, as reported for other proteins and complexes, (iii) bulk photocurrent measurements demonstrate that PSI complexes remain (photo)active upon attachment to the electrode, and (iv) a safe working electrochemical window is identified were PSI activity is retained. These results set the stage for reproducible ECSTM current distance decay experiments in the next section.

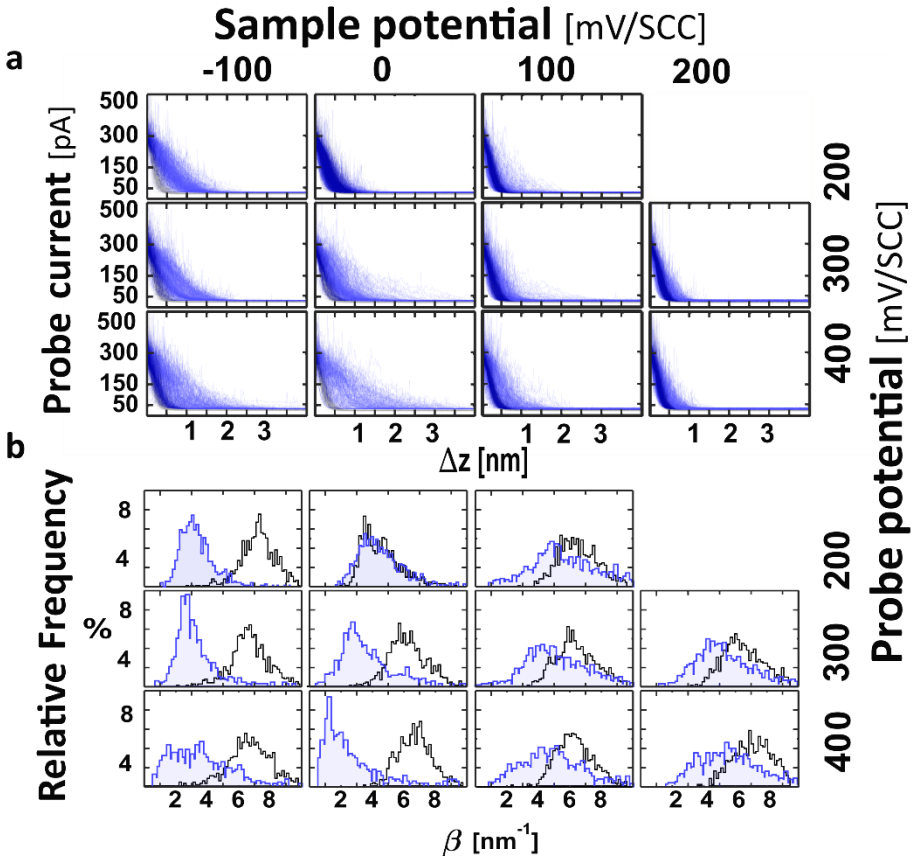

Figure 4. Electrochemical current-distance spectroscopy measurements with ECSTM at different sample and probe potentials: a. Semilogarithmic plots of I(z) recordings of PSI-pIQA-cys-Au samples (blue) and pIQA-cys-Au control (black) at U_S potentials within the safe window for PSI activity and at U_P potentials to probe charge exchange with PSI using moderate bias values. Long distance decay is observed around U_S = 0 mV/SSC and U_P = 400 mV/SSC. **b.** Normalized distribution of β distance-decay rates obtained for each condition in panel a. Low values of β (~1 nm^{-1}) are observed at U_S = 0, U_P = 400 mV/SSC.

Electrochemical current-distance spectroscopy measurements: We used ECSTM to evaluate the distance decay rate of currents in PSI-pIQA-cys-Au samples at fixed locations. The charge exchange process between sample and probe electrodes was measured in dark conditions to prevent photo-oxidation of [28]the P700 site (i.e. in the absence of redox activity of PSI). ECSTM spectroscopy recordings were performed as previously described[28]. Briefly, we departed from a set-point current of 300 pA and switched off the feedback control loop prior to retracting the probe electrode (a Pt-Ir sharp tip) away from the sample electrode (an Au[111] monocrystal, see methods) at a constant rate, while measuring the probe current. Current-distance spectra were recorded under bi-potentiostatic control of probe and sample. We set 11 pairs of potentials for the sample (U_s = -100, 0, 100, 200 mV/SSC) and probe (U_p = 200, 300, 400 mV/SSC) which yield applied bias ranging from +100 mV to +500 mV ($U_{bias} = U_P - U_S$). The positive sign in bias potential was chosen to follow the favored sense of ETp for PSI in dark from stroma to lumen.[21,22]

Logarithmic current plots (Figure 4a) for PSI-pIQA-cys-Au (blue) show longer charge exchange distance with respect to pIQA-cys-Au controls (black). While most control traces are well described by a single exponential decay model, PSI data shows a double exponential behavior (Suppl. Figure S7). Double exponential traces exhibit a short distance regime with z < 0.2 nm (Suppl. Figure S8) and a second regime spanning from 0.2 nm to 1.0 - 2.5 nm depending on the applied probe potential. Beyond 2.5 nm the probe current is masked by faradaic currents (~25 pA) due to probe insulation defects. Double exponential behavior has already been reported for DNA molecules[29] and proteins[30,31] and has been attributed to the surface charge screening[28].

In the absence of PSI, the distribution of β values is centered around 7 nm^{-1} and is independent of potential. In contrast, the β for PSI-pIQA-cys-Au depends both on the sample and probe potentials. At sample potentials above 100 mV/SSC, β is around 4-5 nm^{-1}, similar to previously reported values for Az[28] and PSI complexes.[30] However, at sample potentials equal or below 0 mV/SSC and probe potential 400 mV/SSC we obtained β values below 2 nm^{-1}, which cannot be accounted for by a tunneling mechanism and are reminiscent of the long distance currents observed for C*c*-b*c*$_1$.[31]

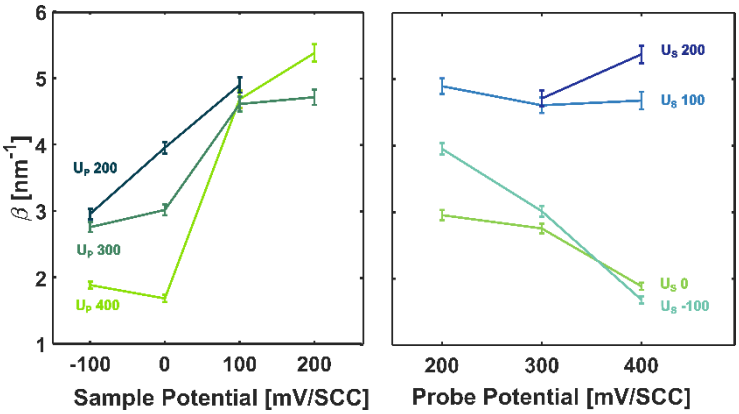

Figure 5. Dependence of the distance decay rate β of PSI-pIQA-cys-Au with the electrochemical potentials. The plots show the statistical representation of β values obtained from Figure 4b in the horizontal (sample potential, left panel) and vertical directions (probe potential, right panel). In the left panel, different probe potentials are indicated in color (U_P = 200, 300, 400 mV/SSC for blue, light green and dark green traces, respectively). In the right panel, constant sample potential traces (U_S =200, 100, 0, -100 mV/SSC) are represented in dark blue, light blue, green and aquamarine, respectively. The lowest rates (corresponding to the farthest-reaching currents) are observed at U_S = 0 mV/SSC and U_P = 400 mV/SSC.

The effect of sample and probe potentials on β distributions (see Suppl. Figure S9) is shown respectively in Figures 5A and 5B. We remark that β values below 4 nm^{-1} are only found for U_S < 100 mV/SSC irrespective of the applied probe potential. Thus, applying a sample potential U_S < 100 mV/SSC is a necessary condition for enhanced charge exchange distance in the dark. Interestingly, bulk photoelectrochemical currents are only observed below this potential (Figure 3). Fulfilled this condition (U_S < 100 mV/SSC), β decreases as the probe potential is increased (Figure 5B). The lowest β values (longest charge exchange distances) are found at U_P = 400 mV/SSC and bias potentials U_{bias} = 500 mV (U_S= 0 mV/SSC) and U_{bias} = 400 mV (U_S = 0 mV/SSC). These results suggest that farthest-reaching currents are due to the probe potential (Fermi energy position around -5.0 eV versus the vacuum level) irrespectively of the applied bias (driving force). The β values as a function of sample and probe electrodes are summarized in Figure 6.

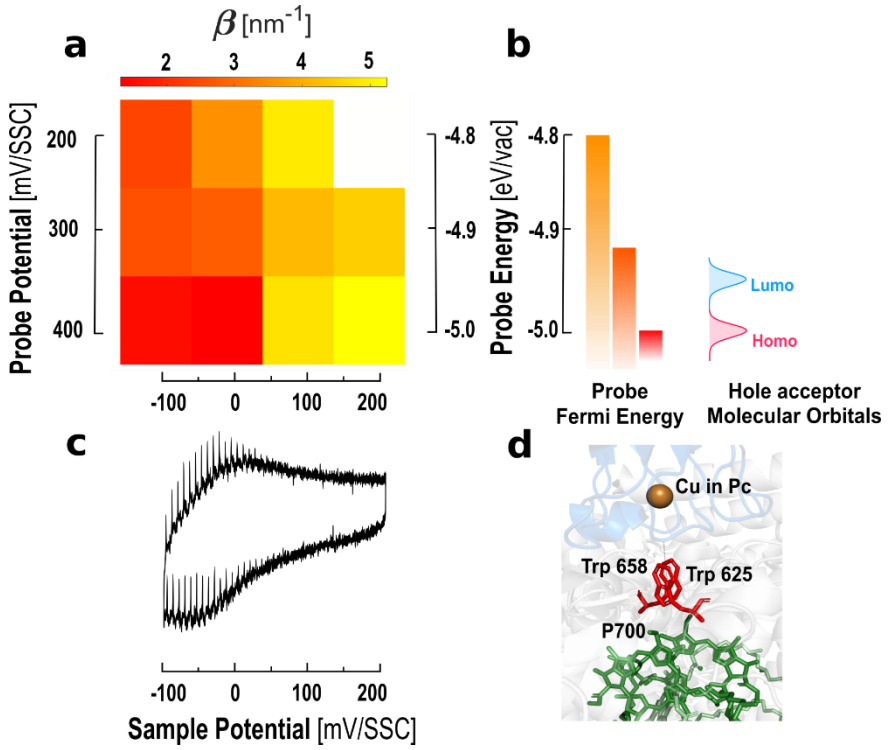

Figure 6. Diagram of distance-decay rates of PSI-pIQA-cys-Au[111] showing electrochemically gated long distance current between the ECSTM probe and the P700 site of PSI in the dark. a. Distance decay rate β average values are plotted in color scale (red corresponding to 2 nm^{-1} and yellow to 5 nm^{-1}) as a function of the probe and sample potentials and using the same layout as Figure 4. **b**. The correspondence of the vertical axis with the electron energy of the probe is shown in the scale on the right, together with a diagram depicting hole injection from the probe at U_P = 400 mV/SSC into a hypothetic electron donor state of PSI in the dark. **c.** A chopped light voltammogram (Figure 3) is indicated under the horizontal axis to show the sample potential range of PSI photo-responses. **d.** Candidate electron donor sites that could mediate this current include a pair of oxidizable tryptophan residues (Trp625, Trp658, shown in red) located between P700 (green) and the copper active site of the PSI redox partner plastocyanin (Pc, orange).

It has been reported that β values in redox proteins[28,30,31] and organic compounds[32] depend on the electrode potentials. In PSI-pIQA-cys-Au, β values depend on the probe rather than on the sample potential (provided that U_S < -100 mV/SSC). We argue that the electric potential at the luminal side of PSI complexes is set by the probe electrode facing the P700 side while the sample potential is screened by pIQA-cys peptide and the 5 nm thick PSI protein matrix. In this sense, the probe electrode can be likened to a PSI redox partner under potentiostatic control.

In these experiments we have focused in ETp through PSI bound to the sample electrode via pIQA-cys peptide and we have avoided ET (redox) effects like direct oxidation of P700 site by carrying out current-distance recordings in dark conditions. However, in contrast to ETp measurements, no direct molecular bond is established between the luminal side of PSI and the ECSTM probe and thus current flow depends to some extent on the aqueous solution, which may involve water molecules and protons as it occurs in ET. This partial electronic decoupling between the electrode and PSI can be seen as an advantage of ECSTM that enabled us to observe gating effects in imaging and spectroscopic experiments of PSI (Figures 3 and 4), as previously found for cytochrome *c* and azurin. It might allow studying the role of electronic coupling between PSI and its partners in the overall ETp process.

We reasoned that the dependence of β on U_P (Figure 6) could be due to the presence of a cofactor or residue on the luminal surface whose molecular orbital could be electronically coupled to the ECSTM probe at 400 mV/SSC (low electron energies). We thus examined the residues on the luminal surface of PSI that could mediate this process, and noticed a pair of tryptophan residues (Trp625 and Trp658 in Figure 4d)[38] that is located in the proximity of P700 and integrates the hydrophobic recognition site of plastocyanin (Pc), an electron donor partner protein of PSI.[51–53] Tryptophan is an oxidizable aromatic residue whose redox activity is involved in photosynthetic water splitting, nucleic acid biosynthesis, and cell signaling, acting as a hole carrier.[54] It plays a major role in proton-coupled electron transfer,[55,56] and it mediates photoinduced long range ET in photolyase[57,58] and in dye-modified Az mutants.[59,60] In plants cryptochrome, the ET rate is modified by two orders of magnitude by ATP binding and by pH modulating the electronic coupling of a Trp residue.[61]

Regarding protein-electrode interfaces, it has been proposed that charge exchange is modulated by electronic coupling between electrode Fermi level and the molecular orbitals of interfacing residues.[16,18,19,44,45,62,63] Remarkably, introducing Trp residues in 6-Alanine peptides increases their molecular conductance, lowering the effective barrier height and enhancing electronic coupling with gold electrodes.[64] In addition, cyclic voltammetry features of Az are abolished if the Trp residue mediating ETp with the electrode is mutated.[65] All these results suggest that aromatic Trp residues play a significant role in protein ET and in ETp. Based in our current-distance spectroscopy results, we hypothesize that surface exposed Trp625 and Trp658 may act as primary electron donors (hole acceptors) to the ECSTM probe, which would explain the gating of the apparent height and β.

The physiological role of Trp residues has been studied in PSI and transient absorption experiments demonstrated that the ET kinetics of PSI with Pc are altered in *Chlamydomonas Reinhardtii* mutants Trp627Phe and Trp651Ser [66,67] (corresponding to Trp625 and Trp658 in *Arabidopsis Thaliana* respectively). In bulk transient absorption measurements, the kinetic contribution of the formation of a productive complex, reorganization, ET, and unbinding processes are indirectly inferred from the different time components of the transient absorption signal. In contrast, distance- and potential-dependent ECSTM experiments allow evaluating the independent contribution of the ET process to the overall charge transport process. Our results suggest that these Trp residues play an additional role as hole exchange mediators in PSI, possibly regulating ET through electronic coupling, in line with findings in other protein systems.

Conclusions

In summary, we have developed a strategy to functionalize gold electrodes with plant PSI complexes that orients and exposes their luminal side to the electrolyte, in order to investigate charge exchange processes mediated by their P700 site. Sample preparation is based on a peptide sequence that binds specifically to the stromal side of PSI from cyanobacteria and plants and it should be applicable to a variety of complexes and substrates. Bulk photoelectrochemical measurements demonstrate that PSI complexes remain fully functional in a wide window around 0 mV/SSC sample potential. Nanoscale imaging of individual complexes shows lateral sizes in agreement with the dimensions of PSI and an apparent height that is electrochemically gated for ECSTM probe potentials around 400 mV/SSC. This experimental setup enables for the first time spectroscopic measurements with ECSTM (current-distance decay at different electrochemical potentials) that unequivocally correspond to the P700 side of PSI exposed to

the aqueous medium. In these conditions, we observe that the spatial span of the current is enhanced (the distance-decay rate β is reduced) through the solution at sample potential 0 mV/SSC and probe potential 400 mV/SSC. This process corresponds to hole injection into an electronic state that is available in the absence of illumination. We propose that a pair of tryptophan residues (Trp625, Trp658) located near P700 and known to integrate the hydrophobic recognition site for Pc may have an additional role as hole exchange mediator involved in the charge transport process through PSI.

Experimental Section:

Arabidopsis thaliana plants (Arabidopsis Col-0) were grown under white light at 120 µmol photons·m^{-2}·s^{-1}, 12 hr/12hr day/night cycle at 23 °C, for 5 weeks. Thylakoid membranes were isolated from Arabidopsis leaves according to *Xu et al.*[68]

PSI-LHCI complexes were purified from thylakoid membranes with sucrose density gradients as previously described.[69] In brief: 350 µg Chl thylakoid were diluted to 0.5 mg Chl·ml^{-1} in 5 mM EDTA, 10 mM Hepes pH 7.5 and solubilized with an equal amount of detergent solution (1% a-DM in 10 mM Hepes 7.5) for 10 min. After solubilization, the sample was centrifuged at 12,000 x g, 10 min centrifugation to eliminate the insolubilized material. The supernatant was loaded onto the sucrose gradients prepared by freezing and thawing a sucrose solution (500 mM sucrose, 20 mM Hepes pH 7.5, 0.06% a-DM). The gradients were centrifuged for 16 hr at 4 °C at 160,000 x g. PSI-LHCI complexes were collected with a syringe.

Sample preparation

Au[111] monocrystals (Mateck GmbH, Germany) were electropolished in H_2SO_4 and flame annealed as previously reported[70]. After annealing, samples were cooled in Ar atmosphere prior to pIQA-cys 0.1 mM incubation in CH_3COONa buffer 50 mM pH 4.5 for 30 min at room temperature. After peptide incubation, samples were gently rinsed with working buffer, Phosphate Buffer Saline (PBS) 50 mM, pH 7.4. Aliquots of 5 µl of PSI samples PSI from WT *Arabidopsis Thaliana*, Chlorophyll concentration 0.28 µg/ul with 0.1% w/w DDM surfactant, isolated from sucrose gradient were incubated with 45 µl of PBS working buffer overnight in dark conditions overnight. After incubation, buffer was gently exchanged with PBS PSI- free buffer to elute unbound complexes. Prior to scanning probe experiments, PSI-pIQA-cys-Au samples were mounted in the ECSTM electrochemical and photo-activity was evaluated. To do so, photo-chronoamperometric recordings (more details in electrochemical characterization methods) were performed at sample potential U_s = -100 mV/SSC in PBS buffer without additional redox mediators (Suppl. Figure S11).

Atomic force microscopy imaging.

AFM scans were performed using an MFP-3D atomic force microscope (Asylum Research, Santa Barbara, CA) using V-shaped Si_3N_4 cantilevers with sharp silicon tips and having a nominal spring constant of 0.12 N·m^{-1} (SNL, Bruker AFM Probes, Camarillo, CA). The AFM was operated in tapping mode in liquid, covering the sample with phosphate buffered saline (PBS) 50 mM, pH 7.4. Set point was adjusted to minimize phase contrast to avoid compressing pIQAC-PSI-monolayer with AFM probe (Suppl. Figure S1)

Electrochemical characterization methods: chopped light cyclic voltammetry and chrono-amperometry:

The homemade electrochemical cell was used for electrochemical characterization in three-electrode configuration and four-electrode configuration for ECSTM. We make use of a miniaturized ultralow leakage membrane Ag/AgCl (SSC) reference electrode filled with 3 M KCl a Pt:Ir (80:20) wire as counter electrode. Cell and all glass material used for preparation of solutions were cleaned with piranha solution (7:3 H_2SO_4/H_2O_2 (30%) by volume). **Caution: Piranha solution should be handled with extreme caution.** Electrochemical measurements were carried out with a potentiostat PGSTAT 302N (Metrohm Autolab, Netherlands). During the photo-chrono-amperometric recordings, the potential was held at U_s = -100 mV/SSC. The sSample was irradiated in 10 s cycles with an LED of 690 nm radiating a power of 20 $mW \cdot cm^{-2}$ in the plane of the sample. Chopped-light cyclic voltammetry experiments were performed at 80 $mV \cdot s^{-1}$ with an irradiation period of 125 ms.

ECSTM-Scans:

PSI-pIQA-cys-Au[111] samples were prepared as described above. For ECSTM imaging, PSI buffer solution containing DDM surfactant 0.1 % w/w was exchanged with DDM free PBS buffer (50 mM, pH 7.4) to complexes with silica beads Zeba spin desalting columns 7kDa (ThermoFischer), since excess of DDM surfactant absorbs on electrode surface hindering protein identification in ECSTM scans[71]. ECSTM probes were prepared cutting Pt-Ir wire with diameter 0.025 mm (GoodFellow, UK) and coated with Apiezon wax to prevent faradaic currents from masking tunnel current. Experiments were performed with a PicoSPM microscope head and a PicoStat bipotentiostat (Molecular Imaging) controlled by Dulcinea electronics (Nanotec Electronica) using WSxM 4.0 software[72]. The applied bias for scans was Ubias= +300 mV and set point current 0.3 nA, resulting in a point conductance of (1.0 10^9 Ω). These parameters have been chosen to position probe electrode at set-point distances avoiding protein squeezing with probe [39]. Sample and probe potentials were set to U_s= -100, -50, 0, 100, 150, 200 mV/SSC and U_P= 200, 250, 300, 400, 450 mV/SSC, respectively. The applied bias is calculated as $U_{bias} = U_P - U_S$. Scan rate was set to 8 Hz acquiring 512 points per line.

ECSTM-Scan blob fitting model:

Scans were analyzed with WsxM 4.0 Software[72] and with a home written program to identify and measure the proteins. The program is based on Adam Ginsburg's gaussfitter (http://github.com/keflavich/gaussfitter) and available at (http://github.com/Mlopeorti/Blob-2D-fitter-). The algorithm fits a 2-dimensional function to scan regions identified manually by the user as molecules. Examples of fit molecules are shown on SI3. Protein lateral size is taken as the full-width-at-half maximum (2.35σ) of the adjusted gaussian. Protein apparent height is obtained as the maximum of the raw data z-piezo position in the selected area.

ECSTM current decay spectroscopy:

Piezo electric nanoprobe positioner was calibrated under experimental conditions taking as reference the Au[111] single atom thick terraces (0.236 nm[73], SI2). Departing from a set point fixed at 0.3 nA, current feedback-loop is switched off and the probe electrode is retracted 10 nm at 40 nm/s. Afterwards, probe is approached again and current-distance feedback loop is reestablished for 400 ms before retracting again. 1000 I(z) curves were recorded for each sample/probe potential pair. To minimize drift artifacts, I-z plots that started with a current deviation higher than 10% of the setpoint were discarded.

Current decay spectroscopy data analysis:

Current-distance curves showing a double exponential behavior[28,29,31,71] were fit with a two-regime exponential function described by the following equation:

$$I(z) = I_{Faradaic} + I_{Set-point} \begin{cases} e^{-\beta_1 z} & for\ z < z_0 \\ e^{-\beta_2 z} e^{z_0(\beta_1 - \beta_2)} & for\ z > z_0 \end{cases}$$

In the model, $I_{Faradiac}$ describe faradaic current term issued from leakage currents due to probe coating defects, this term is obtained as the average of the last 200 points of the I(z) curve. $I_{Set-point}$ is the fixed set point starting current. The fit parameters are β_1 and β_2, the distance decay currents for short and long distance respectively and Z_0 is the point.

The code to analyze I(z) data, written with R software, is available in github repository. https://github.com/Mlopeorti/Tunnel_current_2exponential_fitter/blob/master/2_exp_fit_auto_iz_ECSTM

Acknowledgements.

This research received funding from the European Union Research and Innovation Programme Horizon 2020 – HBP SG3 (945539), DEEPER (ICT-36-2020-101016787), Agency for Management of University and Research Grants/Generalitat de Catalunya (CERCA Programme, 2017-SGR-1442), Fonds Européen de Développement Économique et Régional (FEDER) funds, Ministry of Science and Innovation (Grant PID2019-111493RB- I00, CTQ2015-66194-R). The project CECH, 001-P-001682 is co-financed by the European Union Regional Development Fund within the framework of the ERDF Operational Program of Catalonia 2014-2020 with a grant of 50% of total eligible cost. R.Z. was supported by Becas Chile fellowship 74190117 from the government of Chile.

BIBLIOGRAPHY

(1) Brettel, K. Electron Transfer and Arrangement of the Redox Cofactors in Photosystem I. *Biochimica et Biophysica Acta - Bioenergetics* **1997**, *1318* (3), 322–373. https://doi.org/10.1016/S0005-2728(96)00112-0.

(2) Golbeck, J. H. *Advances in Photosynthesis and Respiration Photosystem I The Light-Driven Plastocyanin:Ferredoxin Oxidoreductase Edited By*.

(3) Croce, R.; van Amerongen, H. Light Harvesting in Oxygenic Photosynthesis: Structural Biology Meets Spectroscopy. *Science*. American Association for the Advancement of Science August 21, 2020. https://doi.org/10.1126/science.aay2058.

(4) Chitnis, P. R. I: Function and Physiology. *Annual Review of Plant Physiology and Plant Molecular Biology* **2001**, *52* (1), 593–626.

(5) Qiu, X.; Castañ, O.; Ocampo, E.; de Vries, H. W.; van Putten, M.; Loznik, M.; Herrmann, A.; Chiechi, R. C. Self-Regenerating Soft Biophotovoltaic Devices. **2018**. https://doi.org/10.1021/acsami.8b11115.

(6) Teodor, A. H.; Bruce, B. D. Putting Photosystem I to Work: Truly Green Energy. *Trends in Biotechnology*. Elsevier Ltd December 1, 2020, pp 1329–1342. https://doi.org/10.1016/j.tibtech.2020.04.004.

(7) Nelson, N. Plant Photosystem I - The Most Efficient Nano-Photochemical Machine. In *Journal of Nanoscience and Nanotechnology*; 2009; Vol. 9, pp 1709–1713. https://doi.org/10.1166/jnn.2009.SI01.

(8) Nakamura, A.; Suzawa, T.; Kato, Y.; Watanabe, T. Species Dependence of the Redox Potential of the Primary Electron Donor P700 in Photosystem i of Oxygenic Photosynthetic Organisms Revealed by Spectroelectrochemistry. *Plant and Cell Physiology* **2011**, *52* (5), 815–823. https://doi.org/10.1093/pcp/pcr034.

(9) Salvatore, P.; Zeng, D.; Karlsen, K. K.; Chi, Q.; Wengel, J.; Ulstrup, J. Electrochemistry of Single Metalloprotein and DNA-Based Molecules at Au(111) Electrode Surfaces. *ChemPhysChem* **2013**, *14* (10), 2101–2111. https://doi.org/10.1002/cphc.201300299.

(10) Zhang, J.; Kuznetsov, A. M.; Ulstrup, J. In Situ Scanning Tunnelling Microscopy of Redox Molecules. Coherent Electron Transfer at Large Bias Voltages. *Journal of Electroanalytical Chemistry* **2003**, *541*, 133–146. https://doi.org/10.1016/S0022-0728(02)01425-0.

(11) Zhang, J.; Chi, Q.; Kuznetsov, A. M.; Hansen, A. G.; Wackerbarth, H.; Christensen, H. E. M.; Andersen, J. E. T.; Ulstrup, J. Electronic Properties of Functional Biomolecules at Metal/Aqueous Solution Interfaces. *Journal of Physical Chemistry B* **2002**, *106* (6), 1131–1152. https://doi.org/10.1021/jp0129941.

(12) Alessandrini, A.; Corni, S.; Facci, P. Unravelling Single Metalloprotein Electron Transfer by Scanning Probe Techniques. *Physical Chemistry Chemical Physics* **2006**, *8* (38), 4383–4397. https://doi.org/10.1039/b607021c.

(13) Chi, Q.; Farver, O.; Ulstrup, J. Long-Range Protein Electron Transfer Observed at the Single-Molecule Level: In Situ Mapping of Redox-Gated Tunneling Resonance. *Proceedings of the National Academy of Sciences of the United States of America* **2005**, *102* (45), 16203–16208. https://doi.org/10.1073/pnas.0508257102.

(14) Bostick, C. D.; Mukhopadhyay, S.; Sheves, M.; Cahen, D.; Lederman, D. Protein Bioelectronics : A Review of What We Do and Do Not Know. 1–150.

(15) Ha, T. Q.; Planje, I. J.; White, J. R. G.; Aragonès, A. C.; Díez-Pérez, I. Charge Transport at the Protein–Electrode Interface in the Emerging Field of

Biomolecular Electronics. *Current Opinion in Electrochemistry* **2021**, *28*, 100734. https://doi.org/10.1016/j.coelec.2021.100734.

(16) Zhang, B.; Song, W.; Brown, J.; Nemanich, R.; Lindsay, S. Electronic Conductance Resonance in Non-Redox-Active Proteins. *Journal of the American Chemical Society* **2020**, *142* (13), 6432–6438. https://doi.org/10.1021/jacs.0c01805.

(17) Zhang, B.; Song, W.; Pang, P.; Lai, H.; Chen, Q.; Zhang, P.; Lindsay, S. Role of Contacts in Long-Range Protein Conductance. *Proceedings of the National Academy of Sciences of the United States of America* **2019**, *116* (13), 5886–5891. https://doi.org/10.1073/pnas.1819674116.

(18) Ron, I.; Sepunaru, L.; Ltzhakov, S.; Belenkova, T.; Friedman, N.; Pecht, I.; Sheves, M.; Cahen, D. Proteins as Electronic Materials: Electron Transport through Solid-State Protein Monolayer Junctions. *Journal of the American Chemical Society* **2010**, *132* (12), 4131–4140. https://doi.org/10.1021/ja907328r.

(19) Lindsay, S. Ubiquitous Electron Transport in Non-Electron Transfer Proteins. *Life*. MDPI AG May 1, 2020. https://doi.org/10.3390/life10050072.

(20) Artés, J. M.; Díez-Pérez, I.; Gorostiza, P. Transistor-like Behavior of Single Metalloprotein Junctions. *Nano Letters* **2012**, *12* (6), 2679–2684. https://doi.org/10.1021/nl2028969.

(21) Castañeda Ocampo, O. E.; Gordiichuk, P.; Catarci, S.; Gautier, D. A.; Herrmann, A.; Chiechi, R. C. Mechanism of Orientation-Dependent Asymmetric Charge Transport in Tunneling Junctions Comprising Photosystem i. *Journal of the American Chemical Society* **2015**, *137* (26), 8419–8427. https://doi.org/10.1021/jacs.5b01241.

(22) Gordiichuk, P.; Pesce, D.; Ocampo, O. E. C.; Marcozzi, A.; Wetzelaer, G.-J. A. H.; Paul, A.; Loznik, M.; Gloukhikh, E.; Richter, S.; Chiechi, R. C.; Herrmann, A. Orientation and Incorporation of Photosystem I in Bioelectronics Devices Enabled by Phage Display. *Advanced Science* **2017**, 1600393. https://doi.org/10.1002/advs.201600393.

(23) van Haeringen, B.; Dekker, J. P.; Bloemendal, M.; Rögner, M.; van Grondelle, R.; van Amerongen, H. Simultaneous Measurement of Electric Birefringence and Dichroism. A Study on Photosystem 1 Particles. *Biophysical Journal* **1994**, *67* (1), 411–417. https://doi.org/10.1016/S0006-3495(94)80496-5.

(24) Wierzbinski, E.; Venkatramani, R.; Davis, K. L.; Bezer, S.; Kong, J.; Xing, Y.; Borguet, E.; Achim, C.; Beratan, D. N.; Waldeck, D. H. The Single-Molecule Conductance and Electrochemical Electron-Transfer Rate Are Related by a Power Law. **2013**. https://doi.org/10.1021/nn401321k.

(25) Langen, R.; Chang, I.-J.; Germanas, J. P.; Richards, J. H.; Winkler, J. R.; Gray, H. B. *Electron Tunneling in Proteins: Coupling Through a P8 Strand*.

(26) Winkler, J. R.; Gray, H. B. Electron Flow through Metalloproteins. *Chemical Reviews* **2014**, *114* (7), 3369–3380. https://doi.org/10.1021/cr4004715.

(27) Chi, Q.; Zhang, J.; Andersen, J. E. T.; Ulstrup, J. Ordered Assembly and Controlled Electron Transfer of the Blue Copper Protein Azurin at Gold (111) Single-Crystal Substrates. *Journal of Physical Chemistry B* **2001**, *105* (20), 4669–4679. https://doi.org/10.1021/jp0105589.

(28) Artés, J. M.; Díez-Pérez, I.; Sanz, F.; Gorostiza, P. Direct Measurement of Electron Transfer Distance Decay Constants of Single Redox Proteins by Electrochemical Tunneling Spectroscopy. *ACS Nano* **2011**, *5* (3), 2060–2066. https://doi.org/10.1021/nn103236e.

(29) He, J.; Lin, L.; Zhang, P.; Lindsay, S. Identification of DNA Basepairing via Tunnel-Current Decay. *NANO LETTERS* **2007**, *7* (12), 3854–3858. https://doi.org/10.1021/nl0726205.

(30) López-Martínez, M.; López-Ortiz, M.; Antinori, M. E.; Wientjes, E.; Nin-Hill, A.; Rovira, C.; Croce, R.; Díez-Pérez, I.; Gorostiza, P. Electrochemically Gated Long-Distance Charge Transport in Photosystem I. *Angewandte Chemie - International Edition* **2019**, *58* (38), 13280–13284. https://doi.org/10.1002/anie.201904374.

(31) Lagunas, A.; Guerra-Castellano, A.; Nin-Hill, A.; Díaz-Moreno, I.; de la Rosa, M. A.; Samitier, J.; Rovira, C.; Gorostiza, P. Long Distance Electron Transfer through the Aqueous Solution between Redox Partner Proteins. *Nature Communications* **2018**, *9* (1), 3–9. https://doi.org/10.1038/s41467-018-07499-x.

(32) Gittins, D. I.; Bethell, D.; Schiffrin, D. J.; Nichols, R. J. *A Nanometre-Scale Electronic Switch Consisting of a Metal Cluster and Redox-Addressable Groups*; 2000.

(33) Leblanc, G.; Gizzie, E.; Yang, S.; Cliffel, D. E.; Jennings, G. K. Photosystem I Protein Films at Electrode Surfaces for Solar Energy Conversion. *Langmuir* **2014**, *30* (37), 10990–11001. https://doi.org/10.1021/la500129q.

(34) Lee, I.; Lee, J. W.; Greenbaum, E. Biomolecular Electronics: Vectorial Arrays of Photosynthetic Reaction Centers. *Physical Review Letters* **1997**, *79* (17), 3294–3297. https://doi.org/10.1103/PhysRevLett.79.3294.

(35) Castañeda Ocampo, O. E.; Gordiichuk, P.; Catarci, S.; Gautier, D. A.; Herrmann, A.; Chiechi, R. C. Mechanism of Orientation-Dependent Asymmetric Charge Transport in Tunneling Junctions Comprising Photosystem i. *Journal of the American Chemical Society* **2015**, *137* (26), 8419–8427. https://doi.org/10.1021/jacs.5b01241.

(36) Mukherjee, D.; May, M.; Vaughn, M.; Bruce, B. D.; Khomami, B. Controlling the Morphology of Photosystem I Assembly on Thiol-Activated Au Substrates. *Langmuir : the ACS journal of surfaces and colloids* **2010**, *26* (20), 16048–16054. https://doi.org/10.1021/la102832x.

(37) Manocchi, A. K.; Baker, D. R.; Pendley, S. S.; Nguyen, K.; Hurley, M. M.; Bruce, B. D.; Sumner, J. J.; Lundgren, C. A. Photocurrent Generation from Surface Assembled Photosystem i on Alkanethiol Modified Electrodes. *Langmuir* **2013**, *29* (7), 2412–2419. https://doi.org/10.1021/la304477u.

(38) Qin, X.; Suga, M.; Kuang, T.; Shen, J. R. Structural Basis for Energy Transfer Pathways in the Plant PSI-LHCI Supercomplex. *Science* **2015**, *348* (6238), 989–995. https://doi.org/10.1126/science.aab0214.

(39) Alliata, D.; Andolfi, L.; Cannistraro, S. Tip to Substrate Distances in STM Imaging of Biomolecules. *Ultramicroscopy* **2004**, *101* (2–4), 231–240. https://doi.org/10.1016/j.ultramic.2004.06.005.

(40) Andolfi, L.; Canters, G. W.; Verbeet, M. P.; Cannistraro, S. Scanning Tunneling Spectroscopy Investigation of Self-Assembled Plastocyanin Mutants onto Gold Substrates under Controlled Environment. *Biophysical Chemistry* **2004**, *107* (2), 107–116. https://doi.org/10.1016/j.bpc.2003.08.012.

(41) Andolfi, L.; Bonanni, B.; Canters, G. W.; Verbeet, M. P.; Cannistraro, S. Scanning Probe Microscopy Characterization of Gold-Chemisorbed Poplar Plastocyanin Mutants. *Surface Science* **2003**, *530* (3), 181–194. https://doi.org/10.1016/S0039-6028(03)00443-6.

(42) Zhang, J.; Chi, Q.; Nielsen, J. U.; Friis, E. P.; Andersen, J. E. T.; Ulstrup, J. Two-Dimensional Cysteine and Cystine Cluster Networks on Au(111) Disclosed by Voltammetry and in Situ Scanning Tunneling Microscopy. *Langmuir* **2000**, *16* (18), 7229–7237. https://doi.org/10.1021/la000246h.

(43) Zhang, J.; Christensen, H. E. M.; Ooi, B. L.; Ulstrup, J. In Situ STM Imaging and Direct Electrochemistry of Pyrococcus Furiosus Ferredoxin Assembled on Thiolate-Modified Au(111) Surfaces. *Langmuir* **2004**, *20* (23), 10200–10207. https://doi.org/10.1021/la048853i.

(44) Garg, K.; Ghosh, M.; Eliash, T.; van Wonderen, J. H.; Butt, J. N.; Shi, L.; Jiang, X.; Zdenek, F.; Blumberger, J.; Pecht, I.; Sheves, M.; Cahen, D. Direct Evidence for Heme-Assisted Solid-State Electronic Conduction in Multi-Heme: C -Type Cytochromes. *Chemical Science* **2018**, *9* (37), 7304–7310. https://doi.org/10.1039/c8sc01716f.

(45) Futera, Z.; Ide, I.; Kayser, B.; Garg, K.; Jiang, X.; van Wonderen, J. H.; Butt, J. N.; Ishii, H.; Pecht, I.; Sheves, M.; Cahen, D.; Blumberger, J. Coherent Electron Transport across a 3 Nm Bioelectronic Junction Made of Multi-Heme Proteins. *Journal of Physical Chemistry Letters* **2020**, *11* (22), 9766–9774. https://doi.org/10.1021/acs.jpclett.0c02686.

(46) Baldacchini, C.; Bizzarri, A. R.; Cannistraro, S. Electron Transfer, Conduction and Biorecognition Properties of the Redox Metalloprotein Azurin Assembled onto Inorganic Substrates. *European Polymer Journal*. Elsevier Ltd October 1, 2016, pp 407–427. https://doi.org/10.1016/j.eurpolymj.2016.04.030.

(47) Yan, J.; Frøkjær, E. E.; Engelbrekt, C.; Leimkühler, S.; Ulstrup, J.; Wollenberger, U.; Xiao, X.; Zhang, J. Voltammetry and Single-Molecule In Situ Scanning Tunnelling Microscopy of the Redox Metalloenzyme Human Sulfite Oxidase. *ChemElectroChem* **2021**, *8* (1), 164–171. https://doi.org/10.1002/celc.202001258.

(48) Zhao, F.; Hardt, S.; Hartmann, V.; Zhang, H.; Nowaczyk, M. M.; Rögner, M.; Plumeré, N.; Schuhmann, W.; Conzuelo, F. Light-Induced Formation of Partially Reduced Oxygen Species Limits the Lifetime of Photosystem 1-Based Biocathodes. *Nature Communications* **2018**, *9* (1). https://doi.org/10.1038/s41467-018-04433-z.

(49) Zhao, F.; Ruff, A.; Rögner, M.; Schuhmann, W.; Conzuelo, F. Extended Operational Lifetime of a Photosystem-Based Bioelectrode. *Journal of the American Chemical Society* **2019**, *141* (13), 5102–5106. https://doi.org/10.1021/jacs.8b13869.

(50) Bennett, T.; Niroomand, H.; Pamu, R.; Ivanov, I.; Mukherjee, D.; Khomami, B. Elucidating the Role of Methyl Viologen as a Scavenger of Photoactivated Electrons from Photosystem i under Aerobic and Anaerobic Conditions. *Physical Chemistry Chemical Physics* **2016**, *18* (12), 8512–8521. https://doi.org/10.1039/c6cp00049e.

(51) Hervás, M.; Navarro, J. A.; de La Cerda, B.; Díaz, A.; de La Rosa, M. A. Reduction of Photosystem I by Cytochrome C6 and Plastocyanin: Molecular Recognition and Reaction Mechanism. *Bioelectrochemistry and Bioenergetics* **1997**, *42* (2), 249–254. https://doi.org/10.1016/S0302-4598(96)05116-1.

(52) Ueda, T.; Nomoto, N.; Koga, M.; Ogasa, H.; Ogawa, Y.; Matsumoto, M.; Stampoulis, P.; Sode, K.; Terasawa, H.; Shimadaa, I. Structural Basis of Efficient Electron Transport between Photosynthetic Membrane Proteins and Plastocyanin in Spinach Revealed Using Nuclear Magnetic Resonance. *Plant Cell* **2012**, *24* (10), 4173–4186. https://doi.org/10.1105/tpc.112.102517.

(53) Hope, A. B. Electron Transfers amongst Cytochrome f, Plastocyanin and Photosystem I: Kinetics and Mechanisms. *Biochimica et Biophysica Acta - Bioenergetics* **2000**, *1456* (1), 5–26. https://doi.org/10.1016/S0005-2728(99)00101-2.

(54) Designed Research; N, A. M. F. P. Defusing Redox Bombs? https://doi.org/10.1073/pnas.1512704112.

(55) Migliore, A.; Polizzi, N. F.; Therien, M. J.; Beratan, D. N. Biochemistry and Theory of Proton-Coupled Electron Transfer. **2014**. https://doi.org/10.1021/cr4006654.

(56) Yee, E. F.; Dzikovski, B.; Crane, B. R. Tuning Radical Relay Residues by Proton Management Rescues Protein Electron Hopping. *J. Am. Chem. Soc* **2019**, *141*, 17571–17587. https://doi.org/10.1021/jacs.9b05715.

(57) Cailliez, F.; Müller, P.; Firmino, T.; Pernot, P.; de La Lande, A. Energetics of Photoinduced Charge Migration within the Tryptophan Tetrad of an Animal (6-4) Photolyase. *Journal of the American Chemical Society* **2016**, *138* (6), 1904–1915. https://doi.org/10.1021/jacs.5b10938.

(58) Martin, R.; Lacombat, F.; Espagne, A.; Dozova, N.; Plaza, P.; Yamamoto, J.; Müller, P.; Brettel, K.; de La Lande, A. Ultrafast Flavin Photoreduction in an Oxidized Animal (6-4) Photolyase through an Unconventional Tryptophan Tetrad. *Physical Chemistry Chemical Physics* **2017**, *19* (36), 24493–24504. https://doi.org/10.1039/c7cp04555g.

(59) Shih, C.; Museth, A. K.; Abrahamsson, M.; Blanco-Rodriguez, A. M.; di Bilio, A. J.; Sudhamsu, J.; Crane, B. R.; Ronayne, K. L.; Towrie, M.; Vlček, A.; Richards, J. H.; Winkler, J. R.; Gray, H. B. Tryptophan-Accelerated Electron Flow through Proteins. *Science* **2008**, *320* (5884), 1760–1762. https://doi.org/10.1126/science.1158241.

(60) Takematsu, K.; Williamson, H. R.; Nikolovski, P.; Kaiser, J. T.; Sheng, Y.; Pospíšil, P.; Towrie, M.; Heyda, J.; Hollas, D.; Záliš, S.; Gray, H. B.; Vlček, A.; Winkler, J. R. Two Tryptophans Are Better Than One in Accelerating Electron Flow through a Protein. *ACS Central Science* **2019**, *5* (1), 192–200. https://doi.org/10.1021/acscentsci.8b00882.

(61) Cailliez, F.; Mu, P.; de la Lande, A. ATP Binding and Aspartate Protonation Enhance Photoinduced Electron Transfer in Plant Cryptochrome. **2014**. https://doi.org/10.1021/ja506084f.

(62) Fereiro, J. A.; Porat, G.; Bendikov, T.; Pecht, I.; Sheves, M.; Cahen, D. Protein Electronics: Chemical Modulation of Contacts Control Energy Level Alignment in Gold-Azurin-Gold Junctions. *Journal of the American Chemical Society* **2018**, *140* (41), 13317–13326. https://doi.org/10.1021/jacs.8b07742.

(63) Yu, X.; Lovrincic, R.; Sepunaru, L.; Li, W.; Vilan, A.; Pecht, I.; Sheves, M.; Cahen, D. Insights into Solid-State Electron Transport through Proteins from Inelastic Tunneling Spectroscopy: The Case of Azurin. *ACS Nano* **2015**, *9* (10), 9955–9963. https://doi.org/10.1021/acsnano.5b03950.

(64) Guo, C.; Yu, X.; Refaely-Abramson, S.; Sepunaru, L.; Bendikov, T.; Pecht, I.; Kronik, L.; Vilan, A.; Sheves, M.; Cahen, D. Tuning Electronic Transport via Hepta-Alanine Peptides Junction by Tryptophan Doping. *Proceedings of the National Academy of Sciences of the United States of America* **2016**, *113* (39), 10785–10790. https://doi.org/10.1073/pnas.1606779113.

(65) Fujita, K.; Nakamura, N.; Ohno, H.; Leigh, B. S.; Niki, K.; Gray, H. B.; Richards, J. H. Mimicking Protein-Protein Electron Transfer: Voltammetry of Pseudomonas Aeruginosa Azurin and the Thermus Thermophilus CuA Domain at ω-Derivatized Self-Assembled-Monolayer Gold Electrodes. *Journal of the American Chemical Society* **2004**, *126* (43), 13954–13961. https://doi.org/10.1021/ja047875o.

(66) Sommer, F.; Drepper, F.; Hippler, M. The Luminal Helix l of PsaB Is Essential for Recognition of Plastocyanin or Cytochrome C6 and Fast Electron Transfer to Photosystem I in Chlamydomonas Reinhardtii. *Journal of Biological Chemistry* **2002**, *277* (8), 6573–6581. https://doi.org/10.1074/jbc.M110633200.

(67) Sommer, F.; Drepper, F.; Haehnell, W.; Hippler, M. The Hydrophobic Recognition Site Formed by Residues PsaA-Trp651 and PsaB-Trp627 of Photosystem I in Chlamydomonas Reinhardtii Confers Distinct Selectivity for Binding of Plastocyanin and Cytochrome c 6. *Journal of Biological Chemistry* **2004**, *279* (19), 20009–20017. https://doi.org/10.1074/jbc.M313986200.

(68) Xu, P.; Tian, L.; Kloz, M.; Croce, R. Molecular Insights into Zeaxanthin-Dependent Quenching in Higher Plants. *Scientific Reports* **2015**, *5* (1), 1–10. https://doi.org/10.1038/srep13679.

(69) Caffarri, S.; Kouřil, R.; Kereïche, S.; Boekema, E. J.; Croce, R. Functional Architecture of Higher Plant Photosystem II Supercomplexes. *EMBO Journal* **2009**, *28* (19), 3052–3063. https://doi.org/10.1038/emboj.2009.232.

(70) Nagy, G.; Wandlowski, T. Double Layer Properties of Au(111)/H 2 SO 4 (Cl) + Cu 2+ from Distance Tunneling Spectroscopy. **2003**. https://doi.org/10.1021/la034950k.

(71) López Martínez, M. Electrochemical Tunneling Microscopy and Spectroscopy of Electron Transfer Proteins. *TDX (Tesis Doctorals en Xarxa)* **2017**.

(72) Horcas, I.; Fernández, R.; Gómez-Rodríguez, J. M.; Colchero, J.; Gómez-Herrero, J.; Baro, A. M. WSXM: A Software for Scanning Probe Microscopy and a Tool for Nanotechnology. *Review of Scientific Instruments* **2007**, *78* (1), 013705. https://doi.org/10.1063/1.2432410.

(73) Spurgeon, P. M.; Lai, K. C.; Han, Y.; Evans, J. W.; Thiel, P. A. Fundamentals of Au(111) Surface Dynamics: Coarsening of Two-Dimensional Au Islands. *Journal of Physical Chemistry C* **2020**, *124* (13), 7492–7499. https://doi.org/10.1021/acs.jpcc.9b12056.